



Supplement of

Projections of leaf area index in earth system models

Natalie Mahowald et al.

Correspondence to: Natalie Mahowald (mahowald@cornell.edu)

The copyright of individual parts of the supplement might differ from the CC-BY 3.0 licence.

1 **Supplemental material:**
2 Sensitivity studies were conducted using the Community Land Model (CLM) (Lawrence et al., 2012), using online model
3 derived meteorology in the CESM-BGC simulations (Lindsay et al., 2014), and using the CLM driven by observed
4 meteorological winds (Qian et al., 2006; Harris et al., 2013). Contrasting these simulations suggest that correlations between
5 LAI and temperature are robust to changing meteorological forcing (Figure S1a and S1b), but that the LAI relationship to
6 precipitation is not robust to changing the input meteorological driving data. (Figure S1c and d) This implies that errors in the
7 simulations of the mean and variability in precipitation in the current climate, that are very difficult for ESMs to simulate well
8 (e.g. Flato et al., 2014), are very important for the simulation of IAV in LAI. Thus we do not include analysis of the LAI to
9 precipitation relationships in the evaluation of the current model simulation.

10 **Supplemental tables**

11 Table S1:Evaluation of LAI over globe. Metrics are described in text and Table 2, models in Table 1.

Models	Mean LAI		Seasonal		Std Dev IAV	LAI IAV correlations	
	Mod el/ob s	Corr.	Std Dev. Model /obs	Avg. Corr.		Model/ obs	LAI vs. Ts
Obs.						0.11	0.21
bcc-csm1	1.74	0.70	1.28	0.54	1.64	-0.07	0.26
bcc-csm1-1	1.52	0.67	1.27	0.55	1.43	-0.13	0.28
BNU-ESM	2.12	0.56	1.47	0.48	1.79	0.27	0.32

CanESM2	1.05	0.66	0.75	0.40	1.15	0.02	0.17
CESM1-BGC	1.49	0.64	0.70	0.48	1.86	0.00	0.24
GFDL-ESM2G	2.27	0.45	0.78	0.18	1.64	-0.06	0.29
GFDL-ESM2M	2.35	0.39	0.78	0.18	1.93	-0.13	0.28
HadGEM2-CC	1.44	0.76	0.58	0.46	0.92	0.15	0.32
HadGEM2-ES	1.52	0.77	0.58	0.46	1.00	0.17	0.35
inmcm4	0.97	0.61	0.93	0.42	0.86	0.05	0.04
IPSL-CM5A-LR	1.44	0.67	0.98	0.49	1.21	0.03	0.08
IPSL-CM5A-MR	1.44	0.68	0.97	0.50	1.21	0.04	0.14
IPSL-CM5B-LR	1.33	0.60	0.95	0.50	1.36	0.02	0.17
MIROC-ESM	1.64	0.44	1.17	0.56	3.23	-0.08	0.11
MIROC-ESM-CHEM	1.62	0.44	1.11	0.53	3.23	-0.05	0.14
MPI-ESM-LR	1.32	0.59	0.83	0.45	0.85	-0.04	0.14
MPI-ESM-MR	1.36	0.60	0.86	0.26	0.85	0.02	0.20
NorESM1-ME	1.61	0.54	0.82	0.44	2.50	-0.05	0.17

1 Table S2a: Tropical LAI evaluation. As in Table S1, but for tropical region (<30°).

Models	Mean LAI		Seasonal		Std Dev IAV	LAI IAV correlations	
	Model/obs	Corr.	Std. Dev. Model/obs	Avg. Corr.		LAI vs. Ts.	LAI vs. Precip..
Obs.						0.02	0.20
bcc-csm1	1.69	0.82	1.79	0.24	2.63	-0.45	0.38
bcc-csm1-1	1.44	0.78	1.66	0.27	2.06	-0.44	0.41
BNU-ESM	2.45	0.63	0.85	0.17	1.25	0.22	-0.04
CanESM2	1.23	0.54	0.74	0.13	1.81	-0.40	0.34
CESM1-BGC	1.72	0.72	0.91	0.38	2.69	-0.29	0.17
GFDL-ESM2G	1.80	0.64	0.96	0.17	2.06	-0.37	0.22
GFDL-ESM2M	1.74	0.63	0.92	0.16	2.50	-0.39	0.24
HadGEM2-CC	1.71	0.81	0.47	0.29	0.88	-0.08	0.28
HadGEM2-ES	1.76	0.81	0.47	0.28	0.94	-0.15	0.33
inmcm4	1.00	0.83	0.83	0.36	0.69	-0.19	0.68
IPSL-CM5A-LR	1.21	0.80	1.09	0.36	1.38	-0.25	0.39
IPSL-CM5A-MR	1.20	0.75	1.09	0.35	1.44	-0.24	0.41
IPSL-CM5B-LR	1.09	0.70	1.02	0.33	1.63	-0.19	0.36
MIROC-ESM	1.61	0.53	0.64	0.35	5.06	-0.37	0.14
MIROC-ESM_CHEM-	1.61	0.53	0.65	0.33	5.00	-0.38	0.15
MPI-ESM-LR	1.41	0.75	1.04	0.15	1.19	-0.51	0.46
MPI-ESM-MR	1.42	0.75	1.06	0.02	1.13	-0.50	0.45
NorESM1-ME	1.73	0.58	0.98	0.32	3.44	-0.34	0.24

2

3

1 Table S2b: Mid-latitude LAI evaluation. As in Table S1, but for mid-latitude region (between 30° and 60°).

	Mean LAI		Seasonal		Std Dev IAV	LAI IAV correlations	
Models	Model/obs	Corr.	Std. Dev. Model/obs	Avg. Corr.	Model/obs	LAI vs. Ts.	LAI vs. time.
Obs.						0.11	0.22
bcc-csm1	1.90	0.60	1.33	0.75	1.50	-0.14	0.23
bcc-csm1-1	1.61	0.52	1.34	0.74	1.50	-0.18	0.31
BNU-ESM	2.20	0.48	1.80	0.61	2.80	0.22	0.07
CanESM2	0.90	0.75	0.88	0.56	1.00	0.03	0.12
CESM1-BGC	1.86	0.73	0.82	0.51	2.80	-0.03	0.09
GFDL-ESM2G	1.37	0.52	1.46	0.17	2.20	-0.07	0.22
GFDL-ESM2M	1.36	0.42	1.37	0.20	2.40	-0.11	0.15
HadGEM2-CC	1.20	0.68	0.86	0.56	1.10	0.02	0.19
HadGEM2-ES	1.21	0.69	0.88	0.57	1.20	0.06	0.23
inmcm4	1.28	0.70	0.83	0.33	1.20	0.15	0.07
IPSL-CM5A-LR	1.68	0.71	1.05	0.53	1.90	0.00	0.05
IPSL-CM5A-MR	1.62	0.76	1.00	0.57	2.00	-0.04	0.09
IPSL-CM5B-LR	1.74	0.69	1.05	0.58	1.80	0.07	0.21
MIROC-ESM	1.89	0.44	1.79	0.71	2.80	-0.09	0.08
MIROC-ESM_CHEM-	1.88	0.46	1.75	0.69	2.80	-0.09	0.08
MPI-ESM-LR	1.42	0.41	0.94	0.71	0.70	0.11	0.07
MPI-ESM-MR	1.47	0.38	0.94	0.52	0.70	0.16	0.15
NorESM1-ME	2.19	0.68	1.09	0.50	3.80	-0.01	0.18

1 Table S2c. High-latitude LAI evaluation. As in Table S1, but for high-latitude region ($> 60^\circ$).

2

	Mean LAI		Seasonal		Std Dev IAV	LAI IAV correlations	
Models	Model /obs	Corr.	Std. Dev. Model/o bs	Avg. Corr.	Model/ obs	LAI vs. Ts.	LAI vs. time
Obs.						0.20	0.21
bcc-csm1	1.73	0.58	0.69	0.91	0.79	0.36	0.43
bcc-csm1-1	1.61	0.57	0.77	0.91	0.86	0.21	0.41
BNU-ESM	1.45	0.35	1.81	0.90	1.93	0.36	0.48
CanESM2	0.85	0.63	0.69	0.74	0.43	0.42	0.31
CESM1-BGC	0.84	0.48	0.35	0.69	0.50	0.31	0.44
GFDL-ESM2G	3.67	0.22	0.21	0.22	1.00	0.26	0.59
GFDL-ESM2M	4.03	0.21	0.23	0.24	1.14	0.11	0.54
HadGEM2-CC	1.13	0.61	0.39	0.70	0.85	0.48	0.58
HadGEM2-ES	1.31	0.60	0.40	0.72	0.92	0.57	0.66
inmcm4	0.71	0.14	1.21	0.79	0.93	0.21	0.08
IPSL-CM5A-	1.68	0.42	0.83	0.71	0.79	0.32	0.27
IPSL-CM5A-	1.74	0.44	0.82	0.72	0.64	0.36	0.31
IPSL-CM5B-	1.50	0.40	0.77	0.75	0.86	0.19	0.25
MIROC-ESM_	1.52	0.31	1.13	0.83	1.00	0.22	0.24
MIROC-ESM-	1.46	0.28	0.97	0.81	1.07	0.29	0.26
MPI-ESM-LR	1.09	0.49	0.56	0.75	0.36	0.32	0.37
MPI-ESM-MR	1.17	0.51	0.56	0.38	0.36	0.43	0.52
NorESM1-ME	0.95	0.38	0.42	0.66	0.71	0.20	0.19

Supplemental Figures

Figure S1: Rank correlation between model derived LAI and temperature (a and b) and precipitation (c and d) for the CESM-BGC (a and c) and for the CLM-obs (b and d). Both models have the same land model, but the difference is that the CESM-BGC meteorology is from the coupled climate model, while the CLM-obs is driven by datasets constrained by observations (Harris et al. 2013; Qian et al. 2006).

Figure S2: Observed distributions of leaf area index (LAI) (units of m^2/m^2) from satellite (Zhu et al. 2013).

Figure S3: Mean of all models for the annual mean change in LAI (m^2/m^2) over time relative to current climate (1981-2000) for 2081-2100 for RCP4.5. (a) The mean change (similar to Figure 1c), (b) the mean change across models normalized by the model standard deviation for 2081-2100 (similar to Figure 2c); and (c) the mean of all models for the fraction of the time during which the annual mean LAI is considered “Low” (model projected annual mean LAI is less than one standard deviation of the current mean at each gridbox) (similar to Figure 5).

Figure S4: Scatter plot of the change in annual average surface temperature (Ts C) (x-axis) against the change in annual average LAI (m^2/m^2) (y-axis) for the global (a), tropics (b), mid-latitudes (c) and high-latitudes (d). Averages over four time periods are shown for each RCP: 1981-2000 (with 0 changes), 2011-2030, 2041-2060 and 2081-2100, connected by a line. The final point (2081-2100) for RCP8.5 is a triangle, while RCP4.5 is a filled circle. The temperatures increase in all simulations with time, so increases in the x-axis indicate an increase in time. Note that there are 4 points along each line, and thus if there is no inflection point, the slope of the line is

constant across the 21st century. This figure is the same as figure 3, but includes RCP4.5.

Figure S5: Probability density function of the change in LAI between 2081-2100 at each grid box for each model for the globe (a), tropics ($<30^\circ$) (b), mid-latitudes (between 30° and 50°) (c) and high-latitudes ($>50^\circ$) (d). The probability density function indicates the fraction of the grid boxes with each LAI value. Probability density functions are smoothed using an Epanechnikov smoothing kernel. Models are show as colored lines, as indicated on legend in figure.

Figure S6: Rank correlation across models at every grid box of the mean model change in LAI (2081-2100 minus 1981-2000) for RCP4.5 against the model change over the same time period of temperature (a) and precipitation (b).

Figure S7: Rank correlation between observational-derived interannual variability in LAI and temperature (a) and year (b) at each grid-box. Correlations above an absolute value of 0.36 are significant at the 95% and are shown in darker colors. Observations are derived from satellite retrievals (Zhu et al., 2013) for LAI and gridded datasets GHCN-CAM (Fan and Dool, 2008) for temperature.

Figure S1

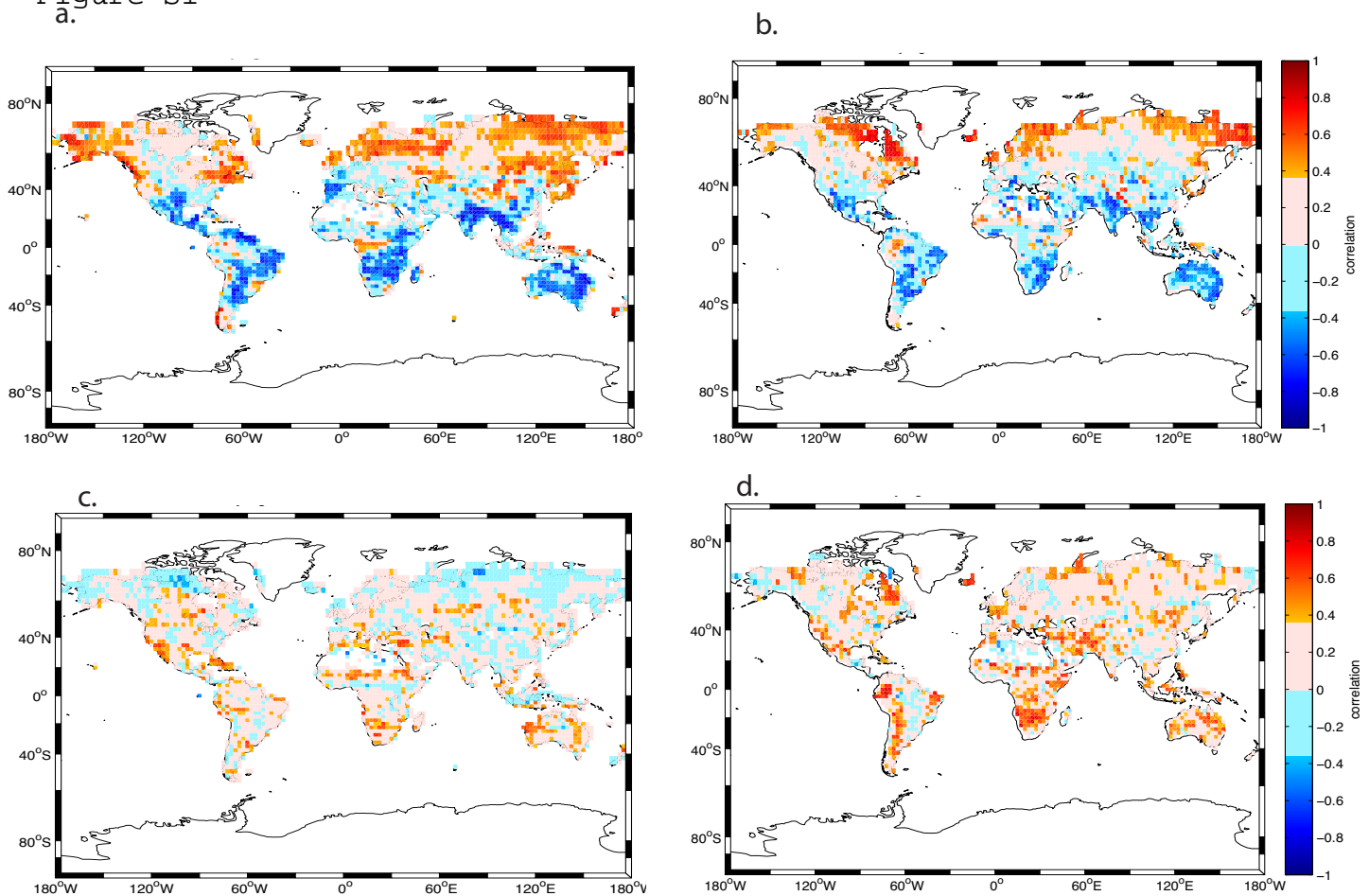


Figure S2

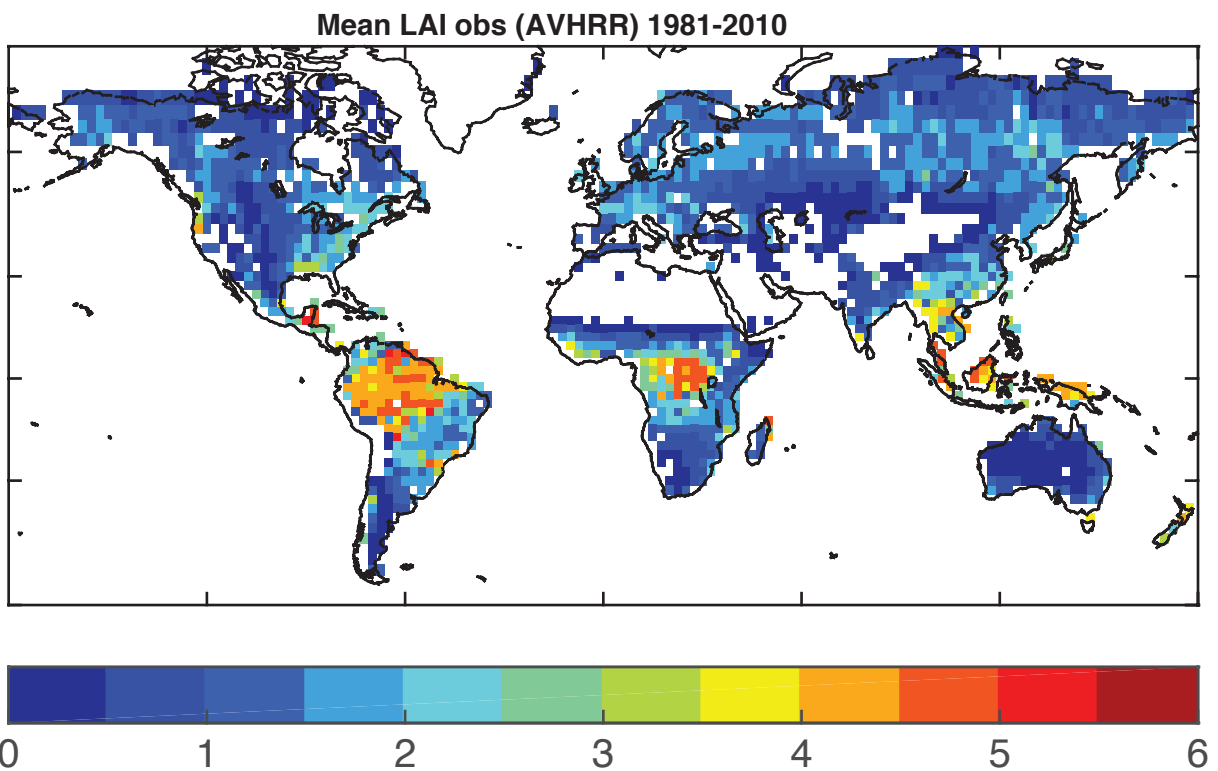
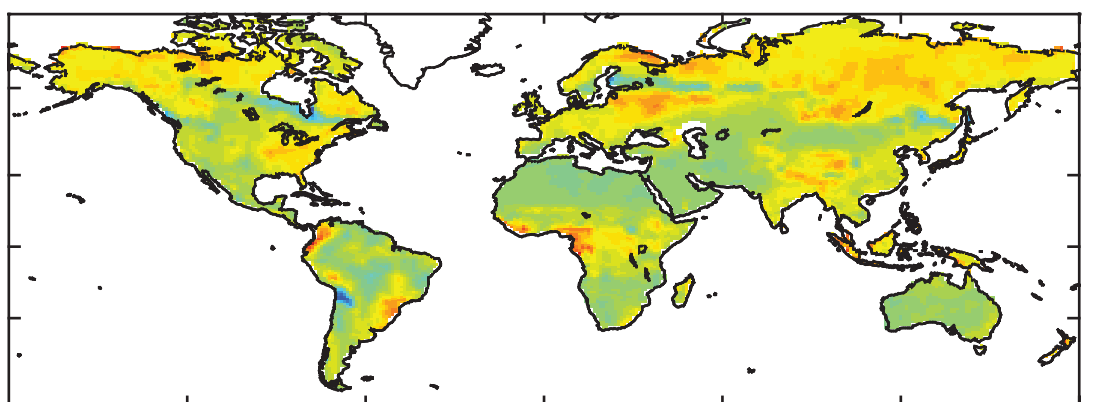
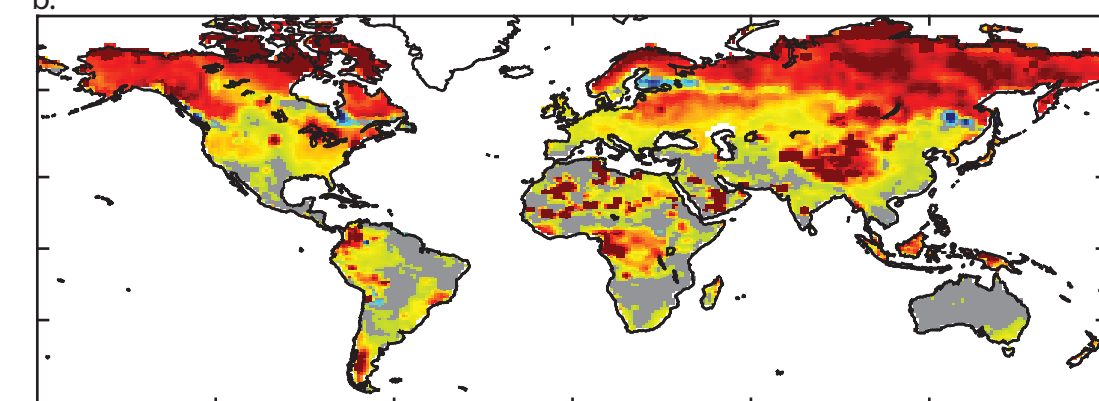


Figure S3

a.



b.



c.

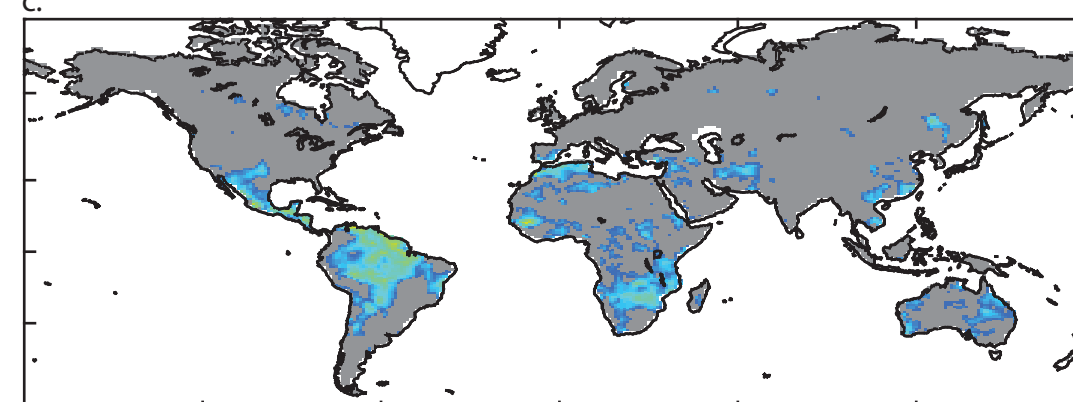
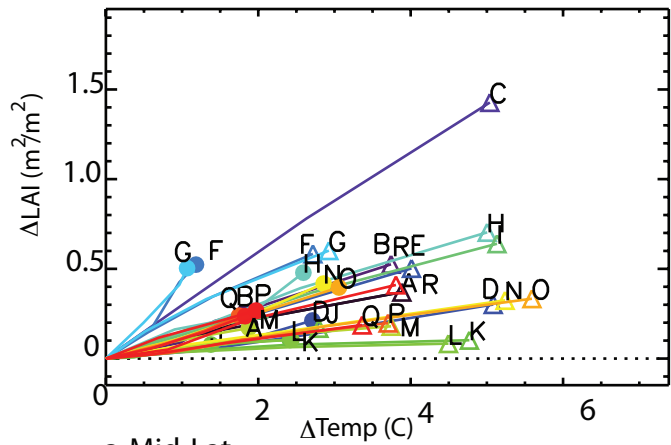
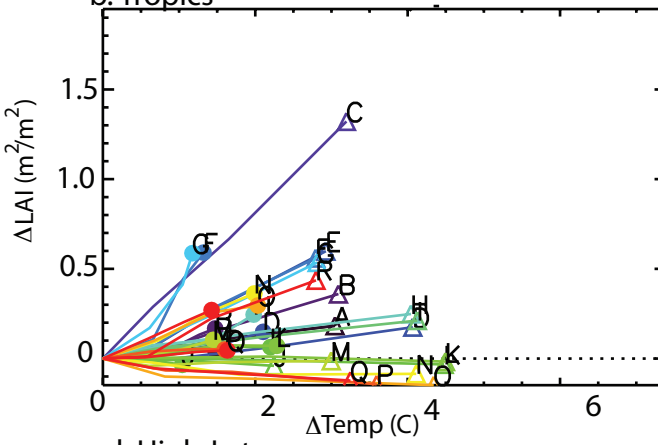


Figure S4

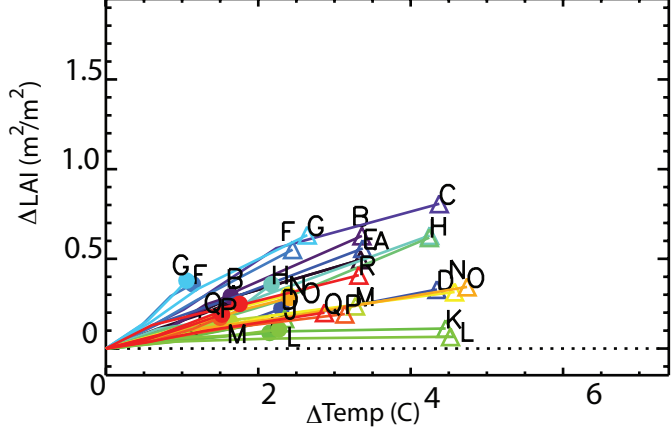
a. Global



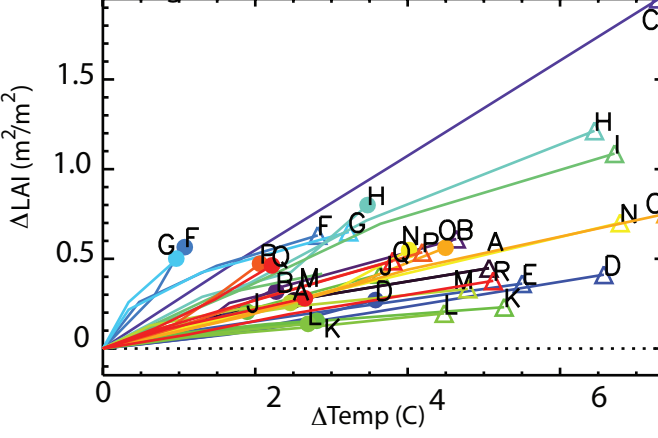
b. Tropics



c. Mid-Lat.



d. High-Lat.



A bcc-csm1-1
B bcc-csm1-1-m
C BNU-ESM
D CanESM2
E CESM1-BGC

F GFDL-ESM2G
G GFDL-ESM2M
H HadGEM2-CC
I HadGEM2-ES
J inmcm4

K IPSL-CM5A-LR
L IPSL-CM5A-MR
M IPSL-CM5B-LR
N MIROC-ESM
O MIROC-ESM-CHEM

P MPI-ESM-LR
Q MPI-ESM-MR
R NorESM1-ME

Figure S5

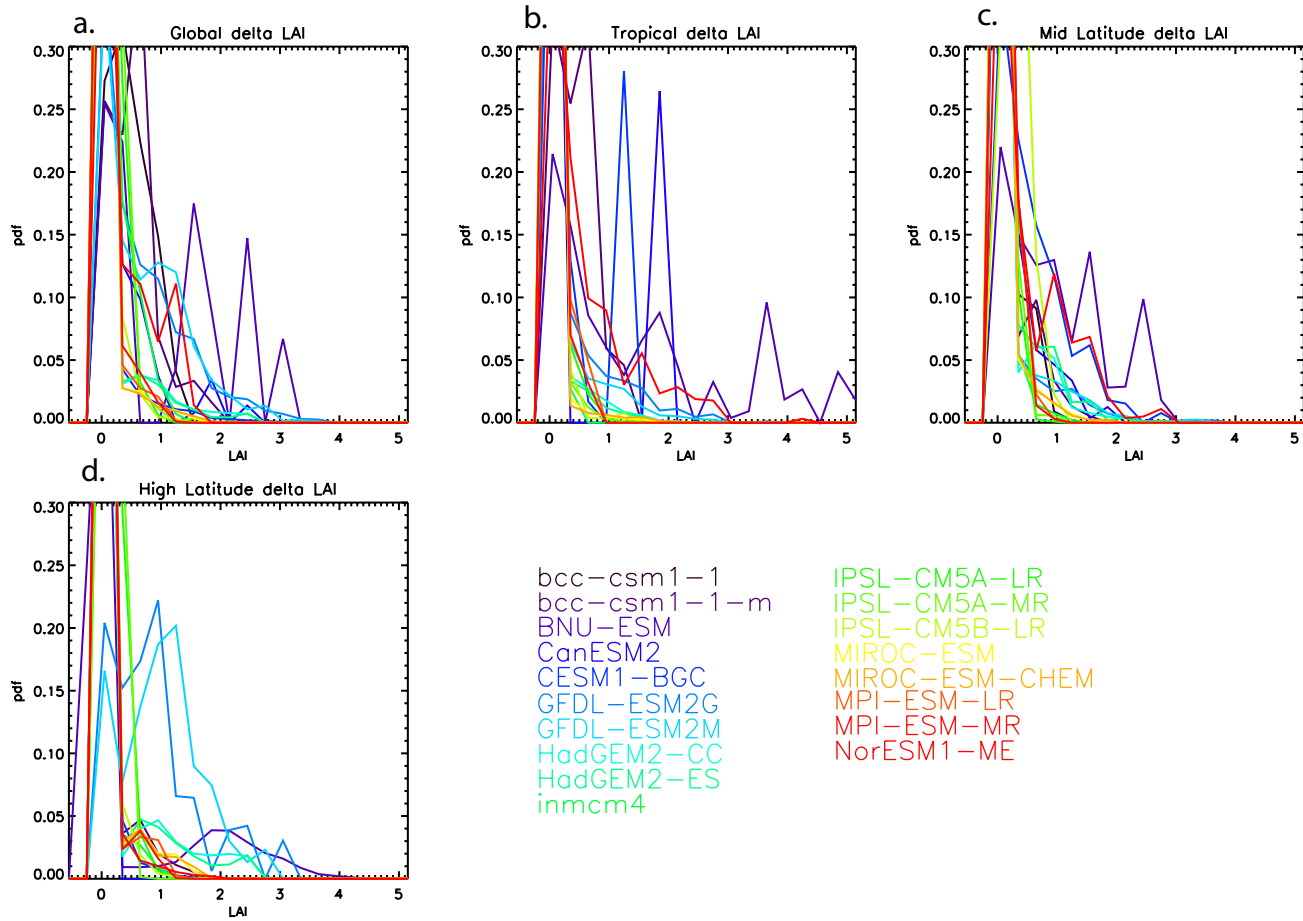
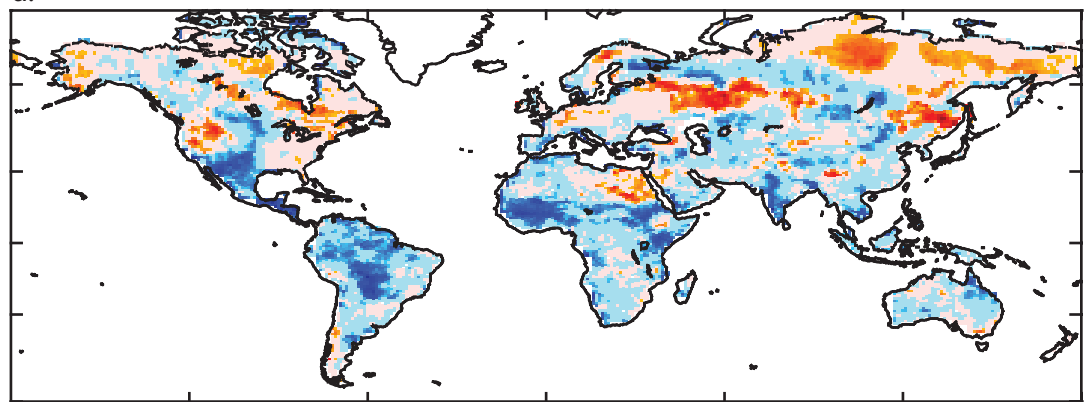


Figure S6

a.



b.

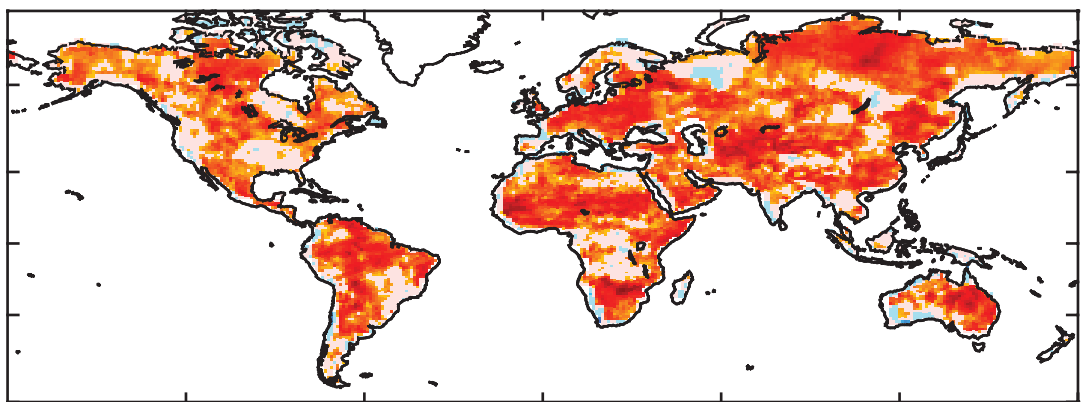
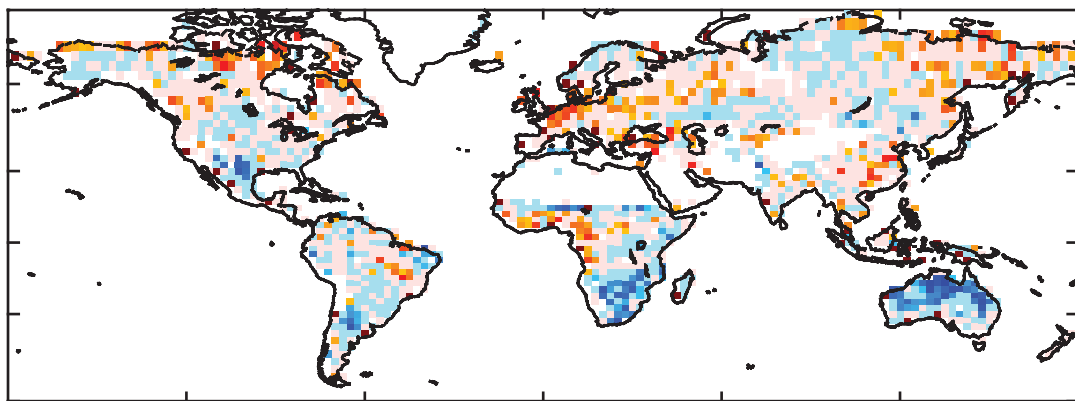


Figure S7

a.



b.

